

Peptidylprolyl isomerase A governs TARDBP function and assembly in heterogeneous nuclear ribonucleoprotein complexes

Eliana Lauranzano,^{1,*} Silvia Pozzi,^{1,*} Laura Pasetto,² Riccardo Stucchi,¹ Tania Massignan,¹ Katia Paoletta,² Melissa Mombrini,² Giovanni Nardo,³ Christian Lunetta,⁴ Massimo Corbo,⁵ Gabriele Mora,⁶ Caterina Bendotti³ and Valentina Bonetto¹

*These authors contributed equally to this work.

Peptidylprolyl isomerase A (PPIA), also known as cyclophilin A, is a multifunctional protein with peptidyl-prolyl *cis-trans* isomerase activity. PPIA is also a translational biomarker for amyotrophic lateral sclerosis, and is enriched in aggregates isolated from amyotrophic lateral sclerosis and frontotemporal lobar degeneration patients. Its normal function in the central nervous system is unknown. Here we show that PPIA is a functional interacting partner of TARDBP (also known as TDP-43). PPIA regulates expression of known TARDBP RNA targets and is necessary for the assembly of TARDBP in heterogeneous nuclear ribonucleoprotein complexes. Our data suggest that perturbation of PPIA/TARDBP interaction causes ‘TDP-43’ pathology. Consistent with this model, we show that the PPIA/TARDBP interaction is impaired in several pathological conditions. Moreover, PPIA depletion induces TARDBP aggregation, downregulates HDAC6, ATG7 and VCP, and accelerates disease progression in the SOD1^{G93A} mouse model of amyotrophic lateral sclerosis. Targeting the PPIA/TARDBP interaction may represent a novel therapeutic avenue for conditions involving TARDBP/TDP-43 pathology, such as amyotrophic lateral sclerosis and frontotemporal lobar degeneration.

- 1 Dulbecco Telethon Institute, IRCCS-Istituto di Ricerche Farmacologiche ‘Mario Negri’, Via La Masa 19, 20156 Milano, Italy
- 2 Department of Molecular Biochemistry and Pharmacology, IRCCS-Istituto di Ricerche Farmacologiche ‘Mario Negri’, Via La Masa 19, 20156 Milano, Italy
- 3 Department of Neuroscience, IRCCS-Istituto di Ricerche Farmacologiche ‘Mario Negri’, Via La Masa 19, 20156 Milano, Italy
- 4 NeuroMuscular Omnicentre (NEMO), Niguarda Cà Granda Hospital, Piazza Ospedale Maggiore, 3, 20162 Milano, Italy
- 5 Department of Neurorehabilitation Sciences, Casa Cura Policlinico, Via Dezza 48, 20144 Milano, Italy
- 6 IRCCS Fondazione Salvatore Maugeri, Via Camaldoli 64, 20138 Milano, Italy

Correspondence to: Valentina Bonetto,
IRCCS-Istituto di Ricerche Farmacologiche ‘Mario Negri’,
Via La Masa 19,
20156 Milano,
Italy
E-mail: valentina.bonetto@marionegri.it

Keywords: cyclophilin A; aggregation; TDP-43; heterogeneous nuclear ribonucleoprotein; RNA metabolism

Abbreviations: ALS = amyotrophic lateral sclerosis; FTL = frontotemporal lobar degeneration; hnRNP = heterogeneous nuclear ribonucleoprotein; PPIase = peptidyl-prolyl *cis-trans* isomerase; PBMC = peripheral blood mononuclear cell

Introduction

Amyotrophic lateral sclerosis (ALS) is an incurable, invariably fatal, neurodegenerative disease causing progressive loss of motor neurons, with muscle paralysis, signs of cognitive impairment in up to half of cases and concomitant frontotemporal lobar degeneration (FTLD) in ~14% of cases (Phukan *et al.*, 2012). ALS is usually classified into two categories: familial ALS (10% of cases), predominantly with autosomal dominant inheritance, and sporadic ALS (90% of cases). Familial ALS has been associated with a number of mutations in several genes, including *SOD1* and *TARDBP*. Although *SOD1* mutations are linked to ~20% of the familial cases, *TARDBP* is mutated in only 4% (Mackenzie *et al.*, 2010). However, inclusions containing the protein encoded by the *TARDBP* gene, (TARDBP, also known as TDP-43), were found in all patients with sporadic ALS and in most familial ALS forms (Neumann *et al.*, 2006; Mackenzie *et al.*, 2007; Sumi *et al.*, 2009). Despite different aetiology, sporadic ALS and familial ALS are clinically indistinguishable, suggesting that the two forms share common pathogenic mechanisms. In the past few years, genetic and neuropathological evidence suggest that an interconnected disruption of protein and RNA homeostasis is possibly at the basis of ALS (Ling *et al.*, 2013; Robberecht and Philips, 2013). The molecular players that should be targeted to halt this deadly process are unknown.

Peptidyl-prolyl isomerase A (PPIA), also known as cyclophilin A, is an abundant, ubiquitously expressed protein, with the highest concentration in the CNS (Ryffel *et al.*, 1991). It is the intracellular ligand of the immunosuppressive drug cyclosporin A and has peptidyl-prolyl *cis-trans* isomerase (PPIase) activity (Fischer *et al.*, 1989), which is linked to its role in protein folding and assembly. Besides the role as a folding catalyst, PPIA has been reported to act as a molecular chaperone (Freskgard *et al.*, 1992). PPIA has been linked to a number of human diseases, but its role in pathogenesis is still unknown (Nigro *et al.*, 2013). We first associated PPIA with nervous system degeneration (Massignan *et al.*, 2007; Nardo *et al.*, 2011) and identified PPIA as hallmark of familial ALS already at a presymptomatic stage in spinal cord of mutant *SOD1* animal models (Massignan *et al.*, 2007; Nardo *et al.*, 2011; Marino *et al.*, 2015). Increased PPIA expression in peripheral blood mononuclear cells (PBMCs) was associated with the disease in patients with sporadic ALS (Nardo *et al.*, 2011). PPIA was also enriched in the detergent-insoluble fraction of spinal cord from mutant *SOD1* mice and post-mortem tissues from sporadic ALS and FTLD patients (Basso *et al.*, 2009; Seyfried *et al.*, 2012). As it is regulated similarly in the mutant-*SOD1* animal models and in sporadic patients, PPIA can be considered a translational biomarker that may suggest common pathogenic mechanisms.

TARDBP (also known as TDP-43) is an RNA binding protein normally localized in the nucleus, whose

physiopathological function is still undefined. Structurally, TARDBP belongs to the heterogeneous nuclear ribonucleoprotein (hnRNP) family, and available evidence suggests that it has multiple roles in RNA processing and gene expression regulation (Buratti and Baralle, 2010). *SOD1* is a well-known cytosolic anti-oxidant enzyme that has been largely studied in connection with ALS. Mutant and/or oxidized misfolded *SOD1* is thought to escape the cell degradation machinery and impair the proteasomal system and autophagy (Bendotti *et al.*, 2012; Chen *et al.*, 2012), inducing a stress response by interfering with various cellular functions. In this work we provide evidence that PPIA is a molecular link between TARDBP and *SOD1* pathologies, and therefore a potential common target for therapeutic intervention.

Materials and methods

Antibodies

Antibodies used for immunoblot (western/dot blot), immunoprecipitation, and immunofluorescence were as follows: rabbit polyclonal anti-human *SOD1* antibody (1:1000 for immunoblot; Millipore), rabbit polyclonal anti-PPIA antibody (1:2500 for immunoblot; 1:300 for immunoprecipitation; Millipore), mouse monoclonal anti-PPIA antibody (1:2000 for immunoblot; 1:250 for immunoprecipitation; 1:500 for immunofluorescence; Abcam), rabbit polyclonal anti-P4HB (1:1000; StressMarq Biosciences Inc.), rabbit polyclonal anti-nitrated actin antibody (1:5000; in house developed; Nardo *et al.*, 2011), mouse monoclonal anti-Myc-tag antibody (1:1000 for immunoblot; 1:100 for immunoprecipitation; OriGene), mouse monoclonal anti-Flag-tag antibody (1:10 000 for immunoblot; 1:200 for immunoprecipitation; Sigma-Aldrich), mouse monoclonal anti-beta actin antibody (1:1000; Santa Cruz Biotechnology), mouse monoclonal anti-lamin A/C antibody (1:500; Millipore), rabbit polyclonal anti-human TDP-43 antibody (1:2500 for immunoblot; 1:300 for immunofluorescence; Proteintech), rabbit polyclonal anti-TDP-43 antibody (1:4000 for immunoblot; 1:500 for immunofluorescence; kindly provided by F. Baralle, ICGEB, Trieste, Italy), mouse monoclonal anti-human phospho Ser409/410 TDP-43 antibody (1:2000 for immunoblot; Cosmo Bio Co., Ltd), rabbit polyclonal anti-ubiquitin (1:800 for immunoblot; Dako), mouse monoclonal anti-HNRNPA2/B1 (1:2000 for immunoblot; 1:200 for immunoprecipitation; Abnova), mouse monoclonal anti-acetyl Lysine (1:500 for immunoblot; 1:200 for immunoprecipitation; Millipore), mouse monoclonal anti-GAPDH (1:10 000 for immunoblot; Millipore), mouse monoclonal anti-SMI-32 antibody (1:3000 for immunofluorescence; Covance), mouse monoclonal anti-tubulin (1:1000 for immunoblot; Sigma-Aldrich), rabbit polyclonal anti-HDAC6 (1:500 for immunoblot; Santa Cruz Biotechnology), rabbit polyclonal anti-ATG7 (1:500 for immunoblot; Thermo Scientific), mouse monoclonal anti-FUS (1:200 for immunoblot; Santa Cruz Biotechnology), rabbit polyclonal anti-POLDIP3 (1:1000 for immunoblot; Cell Signaling), rabbit monoclonal anti-VCP (1:50 000 for immunoblot; Epitomics), rabbit polyclonal anti-human GRN (1:250 for immunoblot; Life Technologies), mouse monoclonal

anti-HA.11 Clone 16B12 (1:200 for immunoprecipitation; Covance), goat anti-mouse or anti-rabbit peroxidase-conjugated secondary antibodies (1:5000 for immunoblot; Santa Cruz Biotechnology Inc.), Qdot800 goat anti-mouse or anti-rabbit IgG-conjugated secondary antibodies (1:1000 for immunoblot; Invitrogen), goat Alexa Fluor® 647 or 594 or 488 anti-mouse or anti-rabbit fluorophore-conjugated secondary antibodies (1:500 for immunofluorescence; Invitrogen).

Cells

Human embryonic kidney epithelial (HEK293) cells were engineered to stably express human SOD1^{WT} or SOD1^{G93A} as described in the Supplementary material. Primary spinal neuron cultures were prepared from spinal cords of Day 14 mouse embryos, as previously described (Basso *et al.*, 2013). SH-SY5Y cells were cultured as described in the Supplementary material.

Animal models

Procedures involving animals and their care were conducted in conformity with institutional guidelines that are in compliance with national (D.L. No. 116, Suppl. 40, Feb. 18, 1992 Circolare No. 8, G.U., 14 luglio 1994) and international laws and policies (EEC Council Directive 86/609. OJ L 358,1, Dec. 12, 1987; NIH Guide for Care and use of Laboratory Animals, U.S. National Research Council, 1996). The characteristics of SOD1^{G93A} mouse lines and controls and the generation of the double transgenic (*SOD1^{G93A}PPIA^{-/-}*) mice and their disease phenotyping are described in the Supplementary material.

Human samples

The study was approved by the ethics committees of the centres involved in the study, IRCCS Fondazione S. Maugeri, NEMO-Niguarda Ca' Granda Hospital, both in Milano, Italy, and the Transfusion Medical Centre at the IRCCS Policlinico S. Matteo, Pavia, and written informed consent was obtained from all participants. The main characteristics of the patients and controls are summarized in the Supplementary material. PBMCs were isolated from blood as previously described (Nardo *et al.*, 2011).

Immunoprecipitation experiments

Magnetic beads coupled with sheep polyclonal antibodies anti-mouse IgG or anti-rabbit IgG (Dynabeads, Invitrogen) were used for co-immunoprecipitation studies. Cells and tissues were lysed in 50 mM Tris-HCl, pH 7.2, 2% CHAPS, 375 U/ml Benzonase® Nuclease (Merck Millipore), protease inhibitor cocktail (Roche) and quantified by the BCA protein assay (Pierce). Proteins (500 µg) were diluted to 0.5 µg/µl with lysis buffer. Magnetic beads with coupled sheep antibodies anti-mouse or anti-rabbit IgG (Dynabeads® M280; Invitrogen) were washed with 0.1% bovine serum albumin (BSA) in PBS to remove preservatives. Approximately 0.1–1 µg Ig/10⁷ beads were incubated for 2 h at 4°C with primary antibodies diluted in 0.1% BSA/PBS as detailed in the 'Antibodies' section. Lysate was pre-cleared by incubation for 2 h at 4°C with the same amount of beads and incubated overnight at 4°C with primary

antibody linked to the beads, in most of the experiments by chemical cross-linking. Cross-linking was done by incubation with 20 mM dimethyl pimelimidate dihydrochloride (Sigma-Aldrich) in 0.2 M triethanolamine pH 8.2 for 30 min at room temperature. Immunoprecipitated proteins were eluted with 50 mM Tris-HCl, pH 6.8, 2% SDS, 100 mM dithiothreitol (DTT) or 100 mM Tris-HCl, pH 6.8, 2% SDS, 10% glycerol and analysed by 2D gel electrophoresis or SDS-PAGE, respectively. For some experiments, HEK293 cells were used in co-immunoprecipitation experiments after pretreatment with 5 µl DNase I (Life Technologies) or 0.2 mg/ml RNase A (Roche) for 15 min at room temperature. All immunoprecipitation experiments were repeated several times on independent sample sets, with consistent results.

Two-dimensional gel electrophoresis

Proteins were dissolved in DeStreak Rehydration Solution (GE Healthcare) added with immobilized pH gradient buffer, pH 3–10, (non-linear) NL 0.5% vol/vol (GE Healthcare), and loaded into 7 cm-immobilized pH gradient strip, pI range, 3–10 NL (GE Healthcare). Isoelectrofocusing was done in an IPGphor apparatus (GE Healthcare) with the following protocol: 30 V for 300 Vh, 200 V for 50 Vh, 2000 V for 2000 Vh, a linear gradient of 3500 V for 2000 Vh, 3500 V for 4000 Vh, a linear gradient of 8000 V for 8000 Vh, 8000 V for 16000 Vh, and forever at 30 V. Strips were reduced with DTT (Sigma-Aldrich) for 15 min and alkylated with iodoacetamide (Sigma-Aldrich) for 15 min. SDS-PAGE was performed by using pre-cast 10% polyacrylamide SDS gel (Invitrogen) and MOPS (Bio-Rad) as running buffer. Gels for 2D western blot were transferred on PVDF membranes (Millipore). Gels for protein identification were fixed overnight in 50% methanol in 7% acetic acid, visualized with Sypro® Ruby Gel Staining (Invitrogen) and scanned with Molecular Imager FX Laser Scanner (excitation, 532 nm; BioRad).

Protein identification

Protein spots were located and excised from 2D gels with the EXQuestTM spot cutter (Bio-Rad). Spots were processed and gel digested with modified trypsin from bovine pancreas (Roche) and identified by mass spectrometry, essentially as previously described (Nardo *et al.*, 2011). Peptide mass fingerprinting and tandem mass spectrometry (MS/MS) were done on a 4800 MALDI TOF/TOF mass spectrometer (Applied Biosystems). The combined MS and MS/MS data were submitted by GPS Explorer v.3.6 software (Applied Biosystems) to the MASCOT database search engine (Version 2.1, Matrix Science) and searched with Uniprot_Swissprot 2011x database. A protein was regarded as identified if the MASCOT protein score, based on the combined MS and MS/MS data, was above the 5% significance threshold for the database (Pappin *et al.*, 1993). Identified proteins were classified on the basis of gene ontology annotations provided by Protein Knowledgebase (UniProtKB).

Total protein extraction

Cell pellets were resuspended in ice-cold lysis buffer: 10 mM Tris-HCl pH 7.5, 0.5% Zwittergent®, 0.5% sodium

deoxycholate, protease inhibitors cocktail (Roche; 1 tablet/10 ml). To disrupt the DNA complexes the sample was passed for ~10 passages through a 26-gauge needle of a 1.5 ml syringe and treated with Benzonase® Nuclease (Merck Millipore) (375 U/ml).

Protein/protein interaction by pull-down analysis

Magnetic beads coated in a cobalt-based surface chemistry (Dynabeads®, Life Technologies) were washed and incubated for 10 min at 4°C with His-TARDBP recombinant protein (Creative BioMart). The coated beads were collected using a magnet and further washed for four times. Recombinant human PPIA (R&D Systems) with and without (UG)₁₀ repeats (Sigma-Aldrich) were prepared in pull-down buffer (3.25 mM sodium phosphate pH 7.4, 70 mM NaCl and 0.01% Tween-20) and incubated with the bead/protein complex for 30 min at room temperature. After four washes with 50 mM sodium phosphate pH 8.0, 300 mM NaCl and 0.01% Tween-20, the beads were collected using a magnet, and Laemmli sample buffer was added before loading onto a 4–15% polyacrylamide gel. Western blot for PPIA was performed to check for the presence of the added recombinant protein. As a control, uncoated beads were used in each experiment.

Subcellular fractionation

HEK293 cells were lysed in RIPA-A buffer (0.3% Triton™ X-100, 50 mM Tris-HCl pH 7.4 and 1 mM EDTA) containing protease inhibitors cocktail (Roche), with rotation at 4°C for 30 min. Cell extracts were centrifuged to pellet nuclei at 12000g at 4°C for 10 min and the supernatant was saved (cytoplasmic fraction). The nuclei pellet was resuspended in RIPA-B buffer (1% Triton™ X-100, 1% SDS, 50 mM Tris-HCl pH 7.4, 500 mM NaCl and 1 mM EDTA) containing protease inhibitors cocktail (Roche). DNA complexes were disrupted using a 1.5-ml syringe and treating with Benzonase® Nuclease (Merck Millipore). Actin and lamin A/C were used as cytosolic and nuclear markers, respectively.

Mouse lumbar spinal cord ventral horns were separated from dorsal horns using a cryostat and homogenized in buffer A (10 mM Tris-HCl pH 7.4, 5 mM MgCl₂, 25 mM KCl, 0.25 M sucrose, 0.5 mM DTT) containing protease inhibitors cocktail (Roche), and centrifuged at 800 g for 10 min at 4°C. The supernatant was centrifuged twice at 800 g for 10 min at 4°C (cytoplasmic fraction). The pellet was resuspended in three volumes of buffer A and centrifuged for three times at 800 g for 10 min at 4°C. The pellet was resuspended in one volume of buffer A and 1 volume of buffer B (10 mM Tris-HCl pH 7.4, 5 mM MgCl₂, 25 mM KCl, 2 M sucrose) containing protease inhibitors cocktail, and loaded on a layer of one volume of buffer B. Samples were ultracentrifuged at 100 000 g for 45 min at 4°C. The pellet (nuclear fraction) was resuspended in 100 µl of buffer A, centrifuged at 800 g for 10 min at 4°C and resuspended in 40 µl buffer A. GAPDH and lamin A/C were used as cytoplasmic and nuclear markers, respectively.

Filter binding assay

The interaction of RNA oligonucleotides with recombinant TARDBP (TDP-43) was assessed by filter binding assay, essentially as previously described (Foster *et al.*, 2011), with some modifications, described in the Supplementary material. Human TARDBP recombinant protein with His-tag at the N-terminus was purchased from Creative BioMart, recombinant PPIA from R&D Systems.

Extraction and analysis of detergent-insoluble and soluble proteins

Mouse tissues were homogenized in 10 volumes (w/v) of buffer, 15 mM Tris-HCl, pH 7.6, 1 mM DTT, 0.25 M sucrose, 1 mM MgCl₂, 2.5 mM EDTA, 1 mM EGTA, 0.25 M sodium orthovanadate, 2 mM sodium pyrophosphate, 25 mM NaF, 5 µM MG132, and protease inhibitors cocktail (Roche; 1 tablet/10 ml), essentially as described (Basso *et al.*, 2009). Samples were centrifuged at 10 000 g at 4°C for 15 min and supernatant 1 was collected in a new tube. The pellet was suspended in ice-cold homogenization buffer with 2% of Triton™ X-100 and 150 mM KCl, sonicated and shaken for 1 h at 4°C. The samples were then centrifuged twice at 10 000 g at 4°C for 10 min to obtain the Triton-resistant fraction pellet and supernatant 2. Supernatants 1 and 2 were pooled, as the Triton-soluble fraction, and analysed by western blot. For the isolation of the Triton-resistant fraction from cell pellets the protocol was slightly modified, as previously described (Basso *et al.*, 2009). The Triton-resistant fraction was resuspended in 7 M urea, 2 M thiourea and 4% CHAPS or 50 mM Tris-HCl pH 6.8, 1 mM DTT and 2% SDS and analysed by dot blot analysis as previously described (Nardo *et al.*, 2011). Densitometry was done with Progenesis PG240 v2006 software (Nonlinear Dynamics). Immunoreactivity was normalized to protein loading (ATX Ponceau S red staining) and multiplied by the amount of Triton-resistant fraction isolated from the tissue/cell pellet (total Triton-resistant fraction), normalized to the soluble protein extracted (Triton-soluble fraction), as quantified by the BCA protein assay (Pierce).

Western blot analysis

Proteins (15–30 µg) after quantification by the BCA protein assay (Pierce) were resuspended in Laemmli sample buffer, separated by electrophoresis on 12% polyacrylamide gels and transferred on PVDF membranes (Millipore), as described (Basso *et al.*, 2009). Blots were probed with primary antibodies according to the manufacturer's protocol and then with peroxidase-conjugated secondary antibodies (Santa Cruz Biotechnology). Blots were developed with Luminata™ Forte Western Chemiluminescent HRP Substrate (Millipore) on the Chemi-Doc XRS System (Bio-Rad). Blots probed with Qdot800-conjugated secondary antibodies were scanned with the Molecular Imager FX Laser Scanner (BioRad). Immunoreactivity was normalized to the actual amount of proteins loaded on the membrane, as detected by ATX Ponceau S red staining solution (Fluka BioChemika). Densitometry was determined with Progenesis PG240 v2006 software (Nonlinear Dynamics).

Immunocytochemistry

Primary spinal neurons were washed with 0.01 M PBS and fixed with 4% paraformaldehyde for 30 min at room temperature. Cells were permeabilized and blocked for non-specific binding in 0.2% Triton™ X-100 (Sigma-Aldrich), 10% normal goat serum (Vector), 0.01 M PBS. Cells were incubated overnight at 4°C with primary antibodies and for 1 h with fluorochrome-conjugated secondary antibodies. For SMI-32 staining, after the incubation with an anti-mouse biotinylated antibody (1:500; Vector), the Tyramide signal amplification system was used (Perkin-Elmer) following the manufacturer's instructions. Confocal microscopy was performed on an Olympus FluoView™ FV1000 microscope.

Molecular biology procedures

Silencing and site-directed mutagenesis were done as described in the Supplementary material.

Results

PPIA interacts with TARDBP and other heterogeneous nuclear ribonucleoproteins

To tackle the complexity of PPIA biology we identified its protein interaction network by a proteomic approach. PPIA-interacting proteins were isolated by immunoprecipitation of PPIA from HEK293 cells, followed by 2D gel electrophoresis and mass spectrometry analysis of co-purified proteins. Cells were used in immunoprecipitation experiments after pretreatment with Benzonase® Nuclease. Figure 1A and B shows representative 2D gel electrophoresis images of the immunoprecipitation fractions from cells silenced or not for PPIA. Silenced cells (Fig. 1B and Supplementary Fig. 1A) served as controls to identify the specific PPIA interactors. The proteins identified are listed in Table 1 and Supplementary Table 1. Gene ontology (GO) analysis of the interactors indicated that PPIA interacts with functionally different groups of proteins (Fig. 1C). The most enriched biological processes are mRNA processing and mRNA splicing that together with mRNA transport amount to 40% of the total. Among PPIA interactors there are several members of the hnRNP family, including TARDBP. HnRNPs are abundant nuclear proteins that shuttle between the nucleus and the cytoplasm and, organized in large complexes, have key roles in multiple steps of mRNA processing. The fact that PPIA interacts with TARDBP confirms its link to pathology and to ALS-FTLD spectrum disorders.

The PPIA and TARDBP interaction is influenced by RNA and PPIase activity

We validated the TARDBP/PPIA interaction by different approaches and in multiple systems. We repeated the co-

immunoprecipitation experiment using an array of controls followed by western blot (Supplementary Fig. 1B), and did the reverse co-immunoprecipitation experiment (Supplementary Fig. 1C). Co-immunoprecipitation and reverse co-immunoprecipitation were also done in cells transfected with Flag-tagged TARDBP and Myc-tagged PPIA (Supplementary Fig. 1D and E). In all cases we confirmed that TARDBP and PPIA specifically associate. Finally, we found that the two proteins can interact directly by pull-down analysis using His-TARDBP-coated beads and recombinant PPIA in the presence or absence of RNA oligonucleotides (Supplementary Fig. 1F). Then, we confirmed the interaction in mouse tissue homogenates (Fig. 2A). In spinal cord of PPIA^{+/-} and PPIA^{-/-} mice there was markedly less co-immunoprecipitated TARDBP, confirming the specificity of the interaction. Immunofluorescence analysis showed that PPIA is highly expressed in neurons (data not shown) and motor neurons (Fig. 2B) and possibly colocalizes with TARDBP in the nucleus. We further investigated the subcellular localization by a biochemical approach. Co-immunoprecipitation from nuclear and cytoplasmic fractions of cells indicated that TARDBP and PPIA interacted mainly in the nucleus (Supplementary Fig. 1G). To test the role of RNA or DNA in the association of these two proteins, cell lysates were subjected to DNase or RNase treatment before co-immunoprecipitation. Removal of RNA, but not of DNA, greatly reduced the interaction between PPIA and TARDBP (Fig. 2C). Similarly, the PPIA/HNRNPA2/B1 interaction was influenced by the presence of RNA (Supplementary Fig. 1H). Finally, a TARDBP mutant lacking the RRM1 domain (Δ 103–183) (TARDBP Δ RRM1), that cannot bind RNA, showed reduced interaction with PPIA (Supplementary Fig. 1I).

The fundamental recognition site for PPIA is a Gly-Pro dipeptide motif (GP-motif) (Yurchenko *et al.*, 2002; Howard *et al.*, 2003; Piotukh *et al.*, 2005). TARDBP has a single GP-motif (residues 348–349) in the C-terminal tail. We used the TARDBP^{G348V} mutant to test whether alteration in the GP-motif affected the interaction. Co-immunoprecipitation experiments were done in cells silenced for endogenous TARDBP and transiently transfected with Flag-tagged wild-type TARDBP or TARDBP^{G348V}. The anti-PPIA antibody did not immunoprecipitate mutant TARDBP (Fig. 2D). The result was the same in the reverse experiment (data not shown). These data indicate that the 348–349 GP-motif might be involved in the interaction. Further studies are required to confirm this indication.

To examine whether the catalytic activity of PPIA was required for the interaction, we ran co-immunoprecipitation experiments in cells transfected with Myc-tagged wild-type PPIA or PPIA^{R55A} deficient in the PPIase activity (Zydowsky *et al.*, 1992). We co-immunoprecipitated less TARDBP from cells expressing PPIA^{R55A}, suggesting that PPIase activity contributes to an efficient interaction (Fig. 2E). Smaller amounts of TARDBP were also recovered from cells treated with cyclosporin A, confirming that PPIase activity is required for interaction (data not shown).

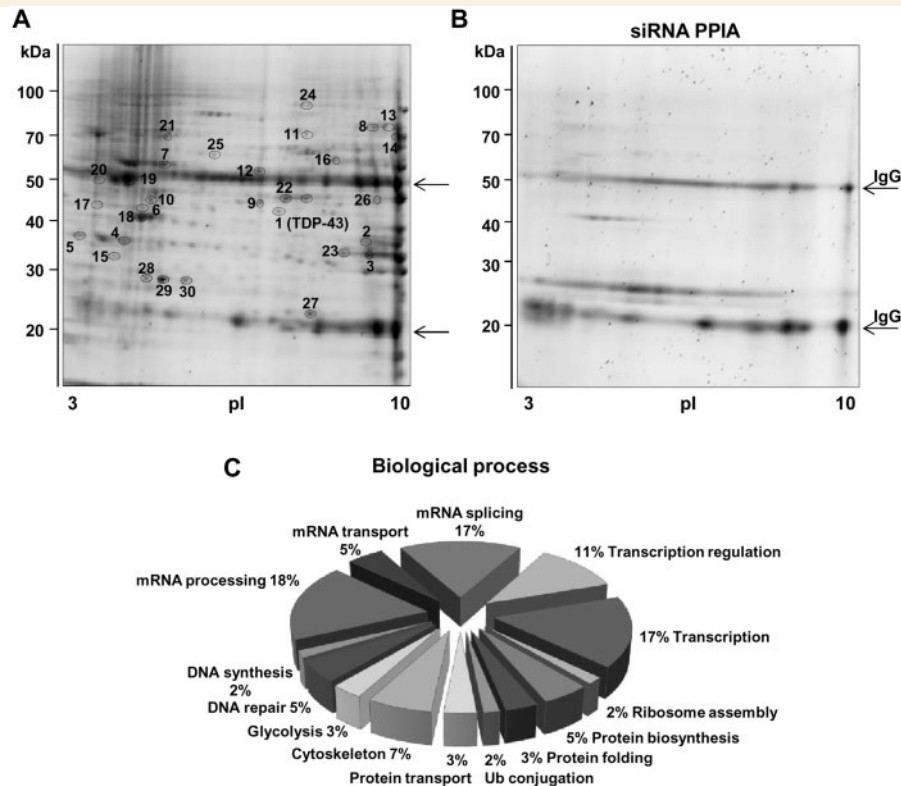


Figure 1 Identification of PPIA-interacting proteins. (A and B) Immunoprecipitation was done using an anti-PPIA polyclonal antibody from HEK293 cells silenced or not for *PPIA*. Cells were used in immunoprecipitation experiments after pretreatment with Benzonase[®] Nuclease. Immunoprecipitate was captured by magnetic beads, separated by 2D gel electrophoresis and stained with Sypro[®] Ruby. Spots in the 2D gel electrophoresis gel from cells silenced for *PPIA* (siRNA *PPIA*) (Supplementary Fig. 1A) were considered contaminants (e.g. the trains of spots indicated are IgG) and the corresponding spots in A were not analysed further. The specific spots were processed and analysed on a 4800 MALDI TOF/TOF mass spectrometer. Spots are labelled with a number and the name of the corresponding identified protein is reported in Table 1. (C) Gene ontology (GO) analysis: the pie chart of the GO terms for biological processes associated with the PPIA interactors. Percentages on slices are calculated as the number of proteins associated with a particular process, normalized to all proteins associated with processes, as 100. See also Supplementary Table 1.

These data indicate that PPIA and TARDBP interact physically in the nucleus and that their interaction is influenced by RNA and PPIA enzymatic activity.

PPIA affects TARDBP-dependent gene expression regulation

TARDBP binds a variety of RNAs and regulates expression and splicing. To investigate the effect of PPIA on TARDBP functions we tested whether depletion of either TARDBP or PPIA have the same effect on a number of known TARDBP targets, such as HDAC6, ATG7, GRN, VCP, FUS and POLDIP3, at a protein level. We confirmed previously published data that loss of TARDBP downregulated HDAC6 and ATG7 and upregulated GRN (Fiesel *et al.*, 2010; Bose *et al.*, 2011; Colombrita *et al.*, 2012) (Fig. 2F and Supplementary Fig. 2A and B). Next, we measured their protein levels after *PPIA* silencing and found that they were reduced or increased to a similar extent as in

TARDBP-silenced cells. These findings indicate that TARDBP and PPIA are required for optimal HDAC6, ATG7 and GRN expression. In the case of HDAC6, simultaneous silencing of *TARDBP* and *PPIA* resulted in a significant additional reduction in HDAC6 expression (Fig. 2F), suggesting that other PPIA substrates may contribute to HDAC6 regulation. We also found that FUS is downregulated in *PPIA*^{-/-} mouse brain as much as in TARDBP-depleted mouse brain (Polymenidou *et al.*, 2011) (Supplementary Fig. 2C). Moreover, VCP, another TARDBP RNA target (Sephton *et al.*, 2011) linked to ALS, is downregulated in *PPIA*^{-/-} mouse brain (Supplementary Fig. 2D). Also in HEK293 cells depletion of TARDBP or PPIA slightly downregulated VCP protein levels (data not shown). Finally, we tested whether PPIA could influence TARDBP activity on *POLDIP3* that upon *TARDBP* silencing is alternatively spliced (Fiesel *et al.*, 2012). Differently from *TARDBP*, *PPIA* silencing did not reduce the main α isoform nor increase the β isoform of *POLDIP3*

Table 1 PPIA protein interactors

Spot ^a	Protein symbol ^b
DNA/RNA binding	
1	TARDBP (TDP-43)
2	HNRNPA1
3	HNRNPA2B1
4-5	HNRNPC
6	RBMXP1
7	HNRNPK
8	HNRNPM
9	EIF4A3
10	EIF4A2 + EIF4A1
11	DDX3X
12	PRPF19
13	SFPQ
14	HKR1
15	NPM1
16	PIAS2
17	NR112
Cytoskeleton-associated	
18	ACTB
19	TUBA1B
20	VIM
21	TMOD2
Energy metabolism	
22	ENO1
23	GAPDH
Others	
24	EEF2
25	TCPI
26	HSPA1A
27	RAN
28-29-30	PHB

^aSpot number as indicated in Fig. 1A.

^bHUGO Gene Nomenclature Committee.

(Supplementary Fig. 2E), indicating that PPIA does not regulate this TARDBP activity.

TARDBP is an RNA binding protein that preferentially binds UG tandem repeats or long clusters of UG-rich motifs. To investigate the mechanism by which PPIA may affect TARDBP functions, we used a filter binding assay to test whether PPIA influenced TARDBP binding to a stretch of 10 UG repeats (UG)₁₀. Constant amounts of (UG)₁₀ and recombinant TARDBP were incubated with increasing concentrations of recombinant PPIA. The addition of PPIA resulted in a dose-dependent increase in the proportion of RNA bound to TARDBP, up to a 20% increase at 150 nM (Fig. 2G). In the absence of TARDBP, PPIA at the highest concentration did not bind RNA. The assay was repeated in the presence of cyclosporin A to test whether PPIase activity was responsible for the increase in binding to (UG)₁₀. Inhibition of the PPIA catalytic activity, and thus of the PPIA/TARDBP interaction, by cyclosporin A decreased TARDBP binding to (UG)₁₀. We concluded that PPIA influences TARDBP binding with (UG)₁₀ through its PPIase activity.

PPIA is necessary for the assembly of TARDBP in heterogeneous nuclear ribonucleoprotein complexes

Analysis of the PPIA interactome indicated that PPIA might be a component of the hnRNP complexes together with TARDBP and other hnRNPs. We found that an anti-HNRNPA2/B1 antibody co-immunoprecipitated PPIA (data not shown) and TARDBP (Fig. 3A). To test whether PPIA has a role in hnRNP complex formation/stabilization we ran co-immunoprecipitation experiments in PPIA-silenced cells and in tissues from PPIA^{-/-} mice. The amount of TARDBP that co-immunoprecipitated with HNRNPA2/B1 was markedly lower in silenced cells and PPIA^{-/-} mice (Fig. 3A and B). To investigate whether PPIA deficiency caused protein complex instability *in vivo* we analysed the Triton-resistant fraction, which is enriched in poly-ubiquitinated, misfolded and damaged proteins (Basso *et al.*, 2006, 2009). Total proteins, ubiquitin, HNRNPA2/B1, TARDBP and aberrantly phosphorylated TARDBP (pTARDBP) were significantly higher in the Triton-resistant fraction from spinal cord (Fig. 3C–F and Supplementary Fig. 3A) and brain cortex (Supplementary Fig. 3B–F) of PPIA^{-/-} mice than PPIA^{+/+} controls. A similar effect was also observed in PPIA-silenced SH-SY5Y cells (Supplementary Fig. 3G and H). These data indicate that PPIA is necessary for hnRNP complex formation and stability.

The PPIA/TARDBP interaction is impaired in amyotrophic lateral sclerosis

Changes in the PPIA/TARDBP interaction may be at the basis of TARDBP/TDP-43 pathology. We therefore examined this interaction in different pathological contexts. The TARDBP G348V pathogenic mutation (Kirby *et al.*, 2010) abolished the interaction with PPIA, possibly by directly affecting the interaction site (Fig. 2D).

To test whether other ALS-associated TARDBP mutations impaired the interaction with PPIA, we did co-immunoprecipitation experiments in cells silenced for endogenous TARDBP and transiently transfected with Flag-tagged TARDBP carrying the A315T, R361S and Y374X mutations (Fig. 4A). The amount of TARDBP that co-immunoprecipitated with PPIA was reduced in the mutant cells (Fig. 4B). The Y374X mutation, which leads to the expression of a C-terminally truncated form of the protein lacking the last 41 amino acids, affected the interaction most, whereas the A315T mutation had the mildest effect.

Next, we analysed the PPIA/TARDBP interaction in PBMCs of patients with ALS. Co-immunoprecipitation was done in PBMC lysates from patients with sporadic ALS and age- and sex-matched healthy controls. TARDBP co-immunoprecipitated with PPIA less efficiently

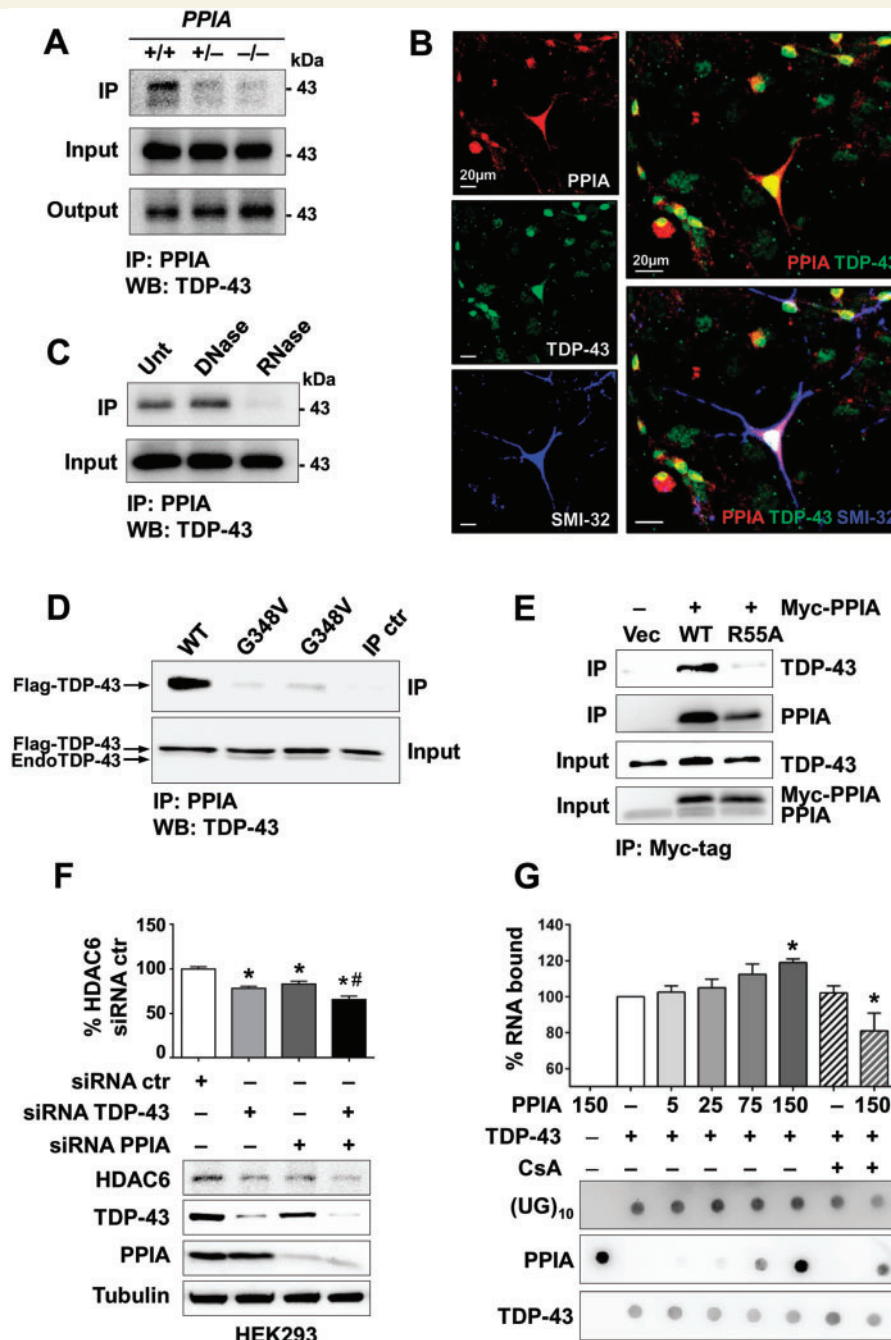


Figure 2 PPIA interacts with TARDBP and regulates its functions. (A) Validation of PPIA/TARDBP interaction in mouse tissues: anti-TARDBP western blot analysis of the immunoprecipitation from homogenates of lumbar spinal cord of *PPIA*^{+/+}, *PPIA*^{+/-} and *PPIA*^{-/-} mice and relative inputs and outputs using an anti-PPIA polyclonal antibody. (B) Representative confocal image of primary spinal neuron cultures co-stained for PPIA (red), TARDBP (green) and motor neuron marker SMI-32 (blue). Scale bar = 20 µm. (C) Immunoprecipitation from cells with an anti-PPIA polyclonal antibody with pretreatment with DNase I (DNase) or RNase A (RNase) or without (Unt). Immunoprecipitation fractions and inputs were analysed by anti-TARDBP western blot. (D) Cells were transiently co-transfected with siRNA for TARDBP (siRNA TDP-43) and Flag-tagged wild-type TARDBP (WT) or Flag-tagged TARDBP carrying the G348V mutation (G348V) (two independent immunoprecipitation experiments are shown). PPIA was co-immunoprecipitated from cells using an anti-PPIA monoclonal antibody followed by anti-TARDBP western blot; immunoprecipitation ctr, magnetic beads linked to the secondary antibody with lysate. (E) Immunoprecipitation from cells transfected with PPIase-deficient PPIA mutant, Myc-tagged PPIA^{R55A} (R55A), Myc-tagged wild-type PPIA (WT) or empty vector (Vec). Immunoprecipitation fractions and inputs were analysed by western blot using anti-PPIA and anti-TARDBP antibodies. (F) HEK293 cells were transiently transfected with siRNA control (siRNA ctr), siRNA TARDBP, siRNA PPIA or both. Western blot for tubulin and HDAC6 showed equal protein loading and specific downregulation after silencing. Immunoreactivity was normalized to protein loading. Data (mean ± SEM, n = 4) are percentages of immunoreactivity in cells silenced with siRNA control. **P* < 0.01 versus siRNA ctr; #*P* < 0.05 versus siRNA TARDBP and siRNA PPIA, by one-way ANOVA, Newman Keuls's *post hoc* test. (G) The influence of PPIA on interaction of TARDBP with (UG)₁₀ was assessed by a filter binding

(continued)

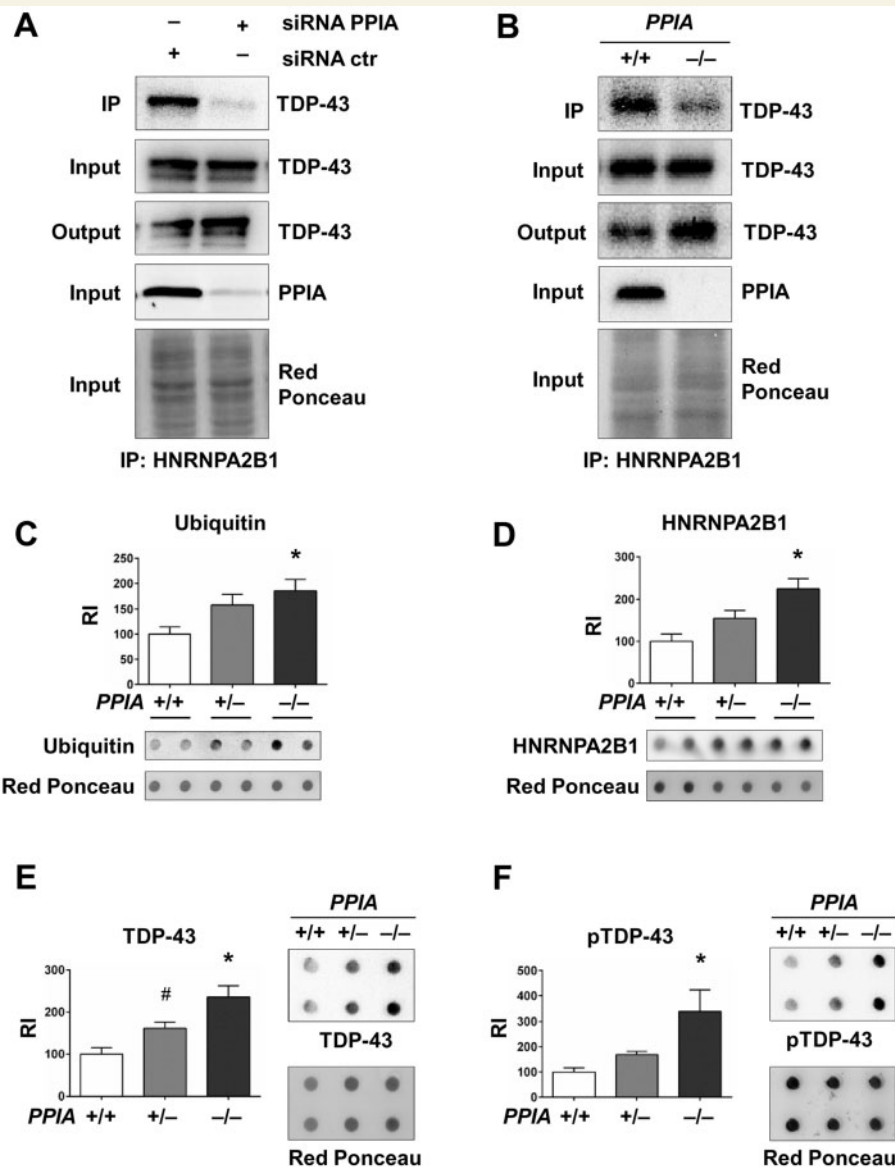


Figure 3 PPIA is necessary for the assembly of TARDBP in hnRNP complexes and their stability. TARDBP (TDP-43) was co-immunoprecipitated using an anti-HNRNPA2/B1 antibody from cells transiently transfected with siRNA PPIA or siRNA control (siRNA ctr) (A) and from spinal cord of *PPIA*^{+/+} and *PPIA*^{-/-} mice (B). Inputs were analysed by western blot with anti-TARDBP antibody for loading control and with anti-PPIA antibody to verify downregulation. (C–F) Analysis of Triton-resistant fraction from ventral horn lumbar spinal cord of *PPIA*^{+/+}, *PPIA*^{+/-} and *PPIA*^{-/-} mice ($n = 6$ per genotype): ubiquitin (C), HNRNPA2/B1 (D), TARDBP (E) and pTARDBP (F) were measured by dot blot with the specific antibodies. Immunoreactivity was normalized to protein loading (Red Ponceau) and multiplied by the amount of Triton-resistant fraction isolated from the tissue. Data (mean \pm SEM, $n = 6$) are percentages of immunoreactivity in *PPIA*^{+/+} mice (RI = relative immunoreactivity). * $P < 0.05$, *PPIA*^{-/-} versus *PPIA*^{+/+}; # $P < 0.05$ *PPIA*^{+/-} versus *PPIA*^{+/+} by one-way ANOVA, Tukey's *post hoc* test. See also Supplementary Fig. 3.

Figure 2 Continued

assay. Biotinylated (UG)₁₀ (500 nM) was premixed with TARDBP (200 nM). Increasing amounts of PPIA (5–150 nM) were then added to the binding reaction, premixed or not with 200 nM cyclosporin A. The TARDBP-bound biotinylated RNA trapped on the nitrocellulose membrane was detected with peroxidase-conjugated streptavidin. In parallel, PPIA and TARDBP were detected with the specific antibodies. RNA bound to TARDBP in all conditions was calculated as a percentage of the control (white bar): TARDBP with (UG)₁₀ in absence of PPIA and cyclosporin A. Data are mean \pm SEM, $n = 6$. * $P < 0.01$ versus control by one-way ANOVA, Sidak's *post hoc* test. See also Supplementary Figs 1 and 2. TDP-43 = TARDBP.

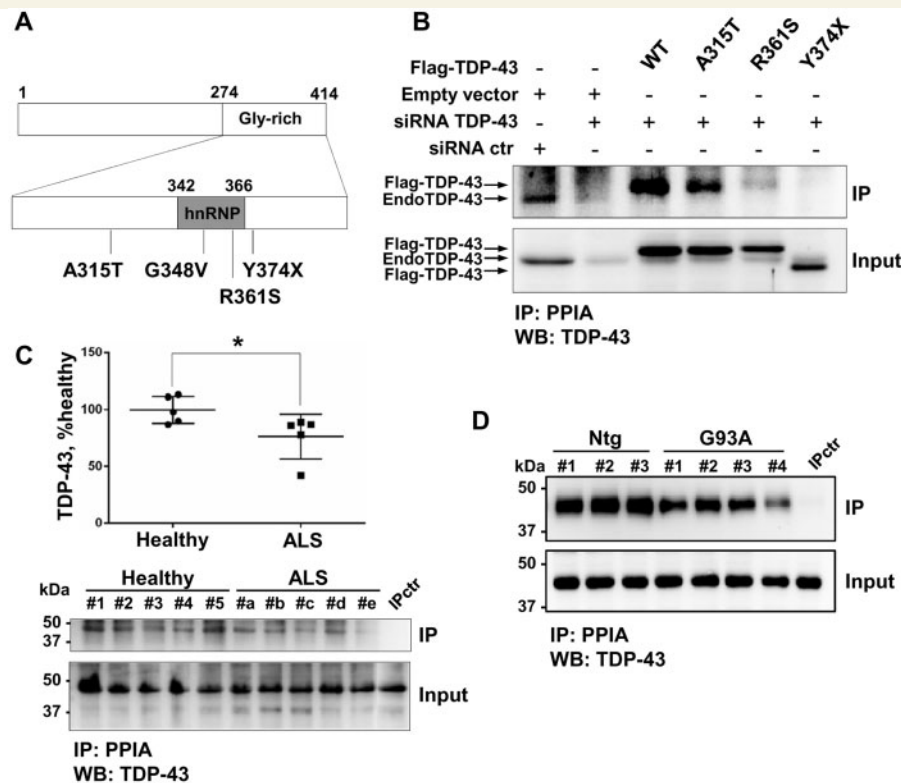


Figure 4 The PPIA/TARDBP interaction is impaired in ALS. (A) Schematic representation of TARDBP protein with the Gly-rich domain (Gly-rich) which has prion-like properties. The ALS-associated mutations introduced in Flag-TARDBP sequence in this study are close to or within the hnRNP binding region (D'Ambrogio *et al.*, 2009; Budini *et al.*, 2012). (B) Cells were transiently co-transfected with siRNA control (siRNA ctr) and an empty vector, or with siRNA for *TARDBP* (siRNA TDP-43) and an empty vector, or with siRNA *TARDBP* and Flag-tagged wild-type TARDBP (WT) or Flag-TARDBP carrying the A315T, R361S or Y374X mutations. PPIA was immunoprecipitated from cells using an anti-PPIA monoclonal antibody and the blot was probed with an anti-TARDBP antibody. (C) TARDBP was co-immunoprecipitated using an anti-PPIA polyclonal antibody from PBMCs of patients with ALS ($n = 5$, ALS) and age- and sex-matched healthy control subjects ($n = 5$, healthy); TARDBP in the immunoprecipitation fractions was normalized to the actual co-immunoprecipitated proteins (Red Ponceau). Scatter plot shows data points and mean \pm SEM, as percentages of healthy controls. * $P < 0.05$ by Student's *t*-test. Immunoprecipitates and inputs were analysed by western blot with a polyclonal anti-TARDBP antibody; immunoprecipitation ctr, magnetic beads linked to the secondary antibody with lysate. (D) TARDBP was co-immunoprecipitated using an anti-PPIA antibody from lumbar spinal cord of non-transgenic ($n = 3$) and SOD1^{G93A} (G93A) ($n = 4$) mice at a presymptomatic stage of the disease (10 weeks of age); immunoprecipitates and inputs were analysed by western blot with an anti-TARDBP antibody; immunoprecipitation ctr, magnetic beads linked to the secondary antibody with lysate. See also Supplementary Fig. 4.

in patients, suggesting less affinity between PPIA and TARDBP also in sporadic ALS (Fig. 4C).

We then tested whether the PPIA/TARDBP interaction was impaired in mutant SOD1 ALS experimental models, where in fact we found TARDBP/TDP-43 pathology, cytoplasmic mislocalization and aggregation (Supplementary Fig. 4A–C). We looked at the PPIA/TARDBP interaction in the lumbar spinal cord of non-transgenic and SOD1^{G93A} mice at a presymptomatic stage of the disease. The anti-PPIA antibody co-immunoprecipitated TARDBP less efficiently in SOD1^{G93A} than in non-transgenic mice (Fig. 4D). Results were similar in HEK293 cells stably expressing SOD1^{G93A} (Supplementary Fig. 4D) that display features previously observed in the spinal cord of mutant SOD1 animal models of ALS (Casoni *et al.*, 2005; Atkin

et al., 2006; Massignan *et al.*, 2007; Nardo *et al.*, 2009, 2011) (Supplementary Fig. 4E–H).

These data indicate an impairment of the PPIA/TARDBP interaction in different pathological contexts that is probably at the basis of TARDBP/TDP-43 pathology.

Lys-acetylation of PPIA favours its interaction with TARDBP and decreases in ALS

We observed changes in the post-translational modification patterns of PPIA in SOD1^{G93A} cells (Supplementary Fig. 4H) and in the spinal cord of the SOD1^{G93A} mice

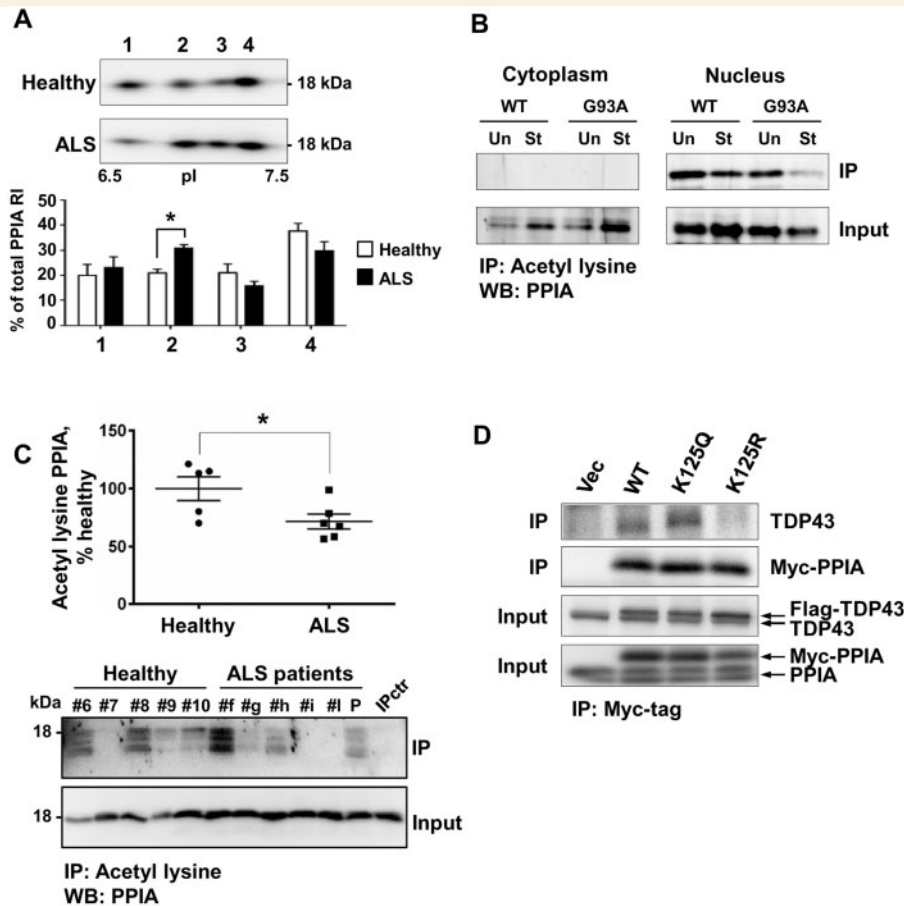


Figure 5 PPIA Lys-acetylation favours PPIA interaction with TARDBP and decreases in ALS. (A) Magnification of a portion of a representative anti-PPIA 2D western blot of PBMC samples from ALS patients (ALS) ($n = 3$) and healthy individuals (Healthy) ($n = 4$). The four PPIA-positive isoforms were quantified as their percentage contribution to the total anti-PPIA immunoreactivity. Data are mean \pm SEM. $*P < 0.01$ versus relative healthy isoform, by Student's t -test. (B) Immunoprecipitation from the cytoplasmic and nuclear fractions of HEK293 SOD1^{WT} (WT) or SOD1^{G93A} (G93A) cells, under basal conditions (Un) and after serum withdrawal (St), using anti-acetyl-lysine antibody. Inputs and immunoprecipitates were analysed by western blot with an anti-PPIA polyclonal antibody. (C) Immunoprecipitation from PBMCs of patients with ALS ($n = 5$, ALS) and age- and sex-matched healthy controls ($n = 5$, healthy) using anti-acetyl-lysine antibody; P is a pool of ALS patients; acetyl-lysine PPIA in the immunoprecipitation fraction was normalized to the total PPIA (input), detected by western blot. Scatter plot shows data points and mean \pm SEM, as percentages of healthy controls; $*P < 0.05$ by Student's t -test. Immunoprecipitates and inputs were analysed by western blot with a polyclonal anti-PPIA antibody; immunoprecipitation ctr, magnetic beads linked to the secondary antibody with lysate. (D) Cells were transfected with the empty vector (Vec), or co-transfected with Flag-TARDBP and Myc-PPIA^{WT} (WT) or Myc-PPIA^{K125Q} (K125Q) or Myc-PPIA^{K125R} (K125R). Myc-PPIA was immunoprecipitated from whole-cell lysates using an anti-Myc-tag antibody and analysed by western blot with anti-TARDBP (top) and an anti-PPIA antibody.

(Massignan *et al.*, 2007). Results were similar in PBMCs of patients with sporadic ALS (Fig. 5A). We hypothesized that changes in PPIA Lys-acetylation could contribute to the different post-translational modification patterns and decrease PPIA affinity for TARDBP.

We characterized PPIA Lys-acetylation in SOD1^{G93A} cells by immunoprecipitation experiments using an anti-acetyl lysine antibody. PPIA was Lys-acetylated exclusively in the nucleus and its acetylation decreased in SOD1^{G93A} cells (Fig. 5B). We also analysed PPIA Lys-acetylation in PBMCs of patients with sporadic ALS and healthy control subjects using the same approach, and detected a lower level in the patients' cells (Fig. 5C).

We therefore explored whether deficient Lys-acetylation influenced the PPIA/TARDBP interaction. We generated two Myc-tagged PPIA mutants at K125: PPIA^{K125Q}, which mimics a constitutively Lys-acetylated PPIA, and PPIA^{K125R} which mimics a constitutively non-acetylated PPIA. Next, we did co-immunoprecipitation experiments using anti-Myc-tag antibody from cells co-transfected with Flag-tagged TARDBP and the different PPIA mutants. TARDBP levels were low in immunoprecipitate from cells transfected with Myc-PPIA^{K125R}, suggesting that this mutant binds TARDBP less efficiently than Myc-PPIA^{WT} and Myc-PPIA^{K125Q} (Fig. 5D). We conclude that Lys-acetylation at K125 favours the PPIA/TARDBP interaction

in the nucleus and that reduced Lys-acetylation of PPIA may contribute to alter the PPIA/TARDBP interaction.

PPIA depletion exacerbates TARDBP/TDP-43 pathology and accelerates disease progression

To test the effect of PPIA depletion on TARDBP/TDP-43 pathology and disease phenotype we crossbred the *PPIA* knockout mouse with the *SOD1^{G93A}* mouse model of ALS (*SOD1^{G93A}PPIA^{-/-}*). We measured the levels of pTARDBP in the Triton-resistant fraction of the ventral horn spinal cord of *SOD1^{G93A}PPIA^{-/-}* mice at the onset and end-stage of disease, and compared them with *SOD1^{G93A}PPIA^{+/+}* mice (Fig. 6A). PPIA depletion raised significantly the levels of insoluble pTARDBP in *SOD1^{G93A}* mice. Increased pTARDBP was also found in brain cortex of *SOD1^{G93A}PPIA^{-/-}* mice (Supplementary Fig. 5). Interestingly, HDAC6, ATG7 and VCP were downregulated in the spinal cord of *SOD1^{G93A}PPIA^{-/-}* mice compared with controls, confirming the effect of PPIA on TARDBP-dependent regulation of gene expression in pathological conditions *in vivo* (Fig. 6G–I). We also found that in the absence of PPIA there was a 2-fold increase of insoluble mutant SOD1 (Supplementary Fig. 6A). Our previous studies indicated that PPIA is sequestered by aggregated SOD1^{G93A} in the spinal cord of *SOD1^{G93A}* mice (Basso *et al.*, 2009). Here we demonstrated that PPIA has a preferential affinity for mutant SOD1 (Supplementary Fig. 6B and C) and probably prevents its aggregation. Accordingly, we showed that *SOD1^{G93A}PPIA^{-/-}* mice have a higher rate of disease progression, as pointed out by the significantly shorter life span and disease duration (Fig. 6B and C, and Supplementary Table 2), slight disease anticipation (Supplementary Table 2), and reduced performance in the functional tests (Fig. 6D–F), indicating that PPIA is a disease modifier.

Discussion

Recently, increasing evidence has indicated that there are important links between RNA metabolism and protein aggregation in a number of degenerative diseases, including several neurodegenerative proteinopathies. Aggregation of the RNA binding protein TARDBP is a key feature in ALS-FTLD spectrum disorders. Converging mechanisms for these disorders have been proposed which imply an interconnected alteration of RNA and protein homeostasis (Ling *et al.*, 2013; Thomas *et al.*, 2013). However, the molecular mechanisms underlying TARDBP/TDP-43 pathology are not yet known.

Here we report that PPIA interacts with TARDBP in the nucleus, that the interaction is influenced by the presence of RNA and PPIA enzymatic activity, and is favoured by Lys-acetylation. PPIA regulates TARDBP activities and is

necessary for the assembly of TARDBP in hnRNP complexes and their stability. We also provide evidence that PPIA depletion induces TARDBP aggregation and accelerates disease progression in a mutant SOD1 mouse model of ALS. Finally, the PPIA/TARDBP interaction is impaired in several pathological conditions, including sporadic ALS. On the basis of these findings we propose a unifying model to explain TARDBP/TDP-43 pathology (Fig. 7). In physiological conditions, PPIA is part of hnRNP complexes together with TARDBP and other hnRNPs and regulates their structure, which undergoes highly dynamic rearrangements involving binding and dissociation during mRNA biogenesis (Dreyfuss *et al.*, 2002). In pathological conditions, mutant TARDBP and/or PPIA deacetylation and/or PPIA accidental sequestration into aggregates, while acting as a molecular chaperone, lead to a looser PPIA/TARDBP interaction. This induces dissociation and instability of the hnRNP complexes, TARDBP mislocalization and aggregation in the cytoplasm. An altered PPIA/TARDBP interaction may affect TARDBP-dependent regulation of genes, such as HDAC6, ATG7 and VCP that are involved in clearance of protein aggregates thus contributing to worsen disease phenotype. A similar mechanism can be envisaged in the presence of HNRNPA2/B1 and HNRNPA1 mutations, which are associated with multisystem proteinopathy marked by prominent TARDBP/TDP-43 pathology (Kim *et al.*, 2013). In this case an altered PPIA/hnRNPs interaction would induce hnRNP complex instability and TARDBP aggregation. We suggest that this novel function of PPIA within hnRNP complexes has important implications for several pathological conditions involving TARDBP/TDP-43 pathology.

PPIA plays a key role in the assembly and dynamics of heterogeneous nuclear ribonucleoprotein complexes

PPIA co-immunoprecipitates with proteins that regulate mRNA splicing, transport and stability, such as several hnRNPs, including TARDBP. PPIA was previously identified as a putative TARDBP interactor in a global proteomic analysis, but the interaction was disregarded as non-specific (Freibaum *et al.*, 2010). We have now demonstrated the specificity of the interaction and identified possible functional implications.

TARDBP is an integral component of hnRNP complexes (D'Ambrogio *et al.*, 2009; Freibaum *et al.*, 2010), and binds hnRNPs through its C-terminal tail (Buratti *et al.*, 2005); HNRNPA2/B1 is the major hnRNP recognized by TARDBP (Buratti *et al.*, 2005). In our proteomic analysis HNRNPA2/B1 interacted with PPIA, confirming previous observations (Pan *et al.*, 2008). We also obtained evidence that PPIA has a fundamental role in the interaction of TARDBP with HNRNPA2/B1. Thus, PPIA, TARDBP and HNRNPA2/B1 may interact with each other, and PPIA be a component of the hnRNP-rich particles. The molecular

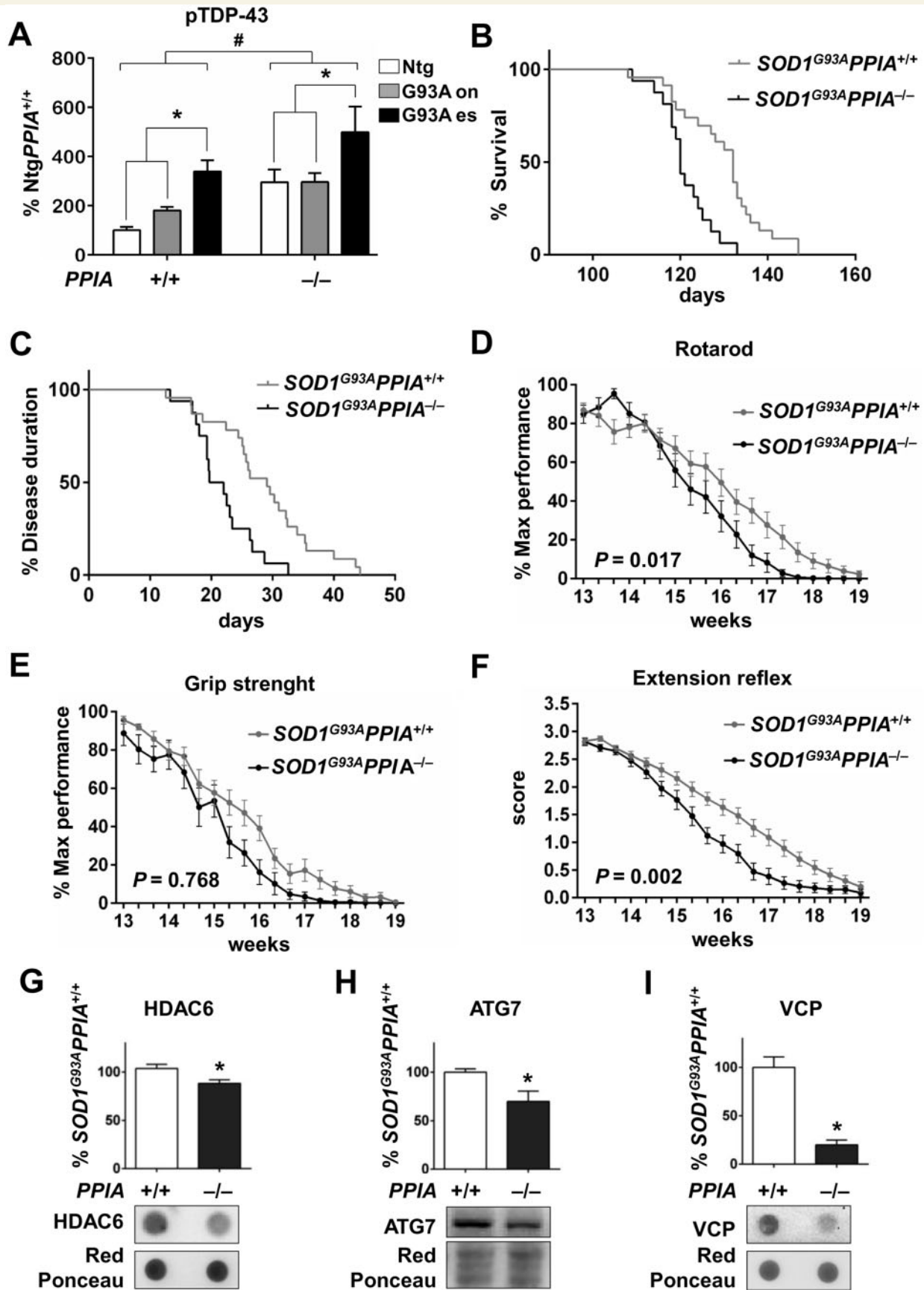


Figure 6 PPIA depletion exacerbates TARDBP pathology and accelerates disease progression. (A) Dot blot analyses of Triton-resistant fraction from ventral horn lumbar spinal cord tissues of $SOD1^{G93A}$ and non-transgenic (Ntg) mice expressing (+/+) or not (-/-) PPIA at

(continued)

details of this putative complex were not determined and await further studies.

Our findings raise the possibility that PPIA plays a key role in the architecture of the RNA-binding protein complexes. In fact, depletion of PPIA in mice impaired the assembly of the hnRNP complexes in the spinal cord and brain cortex, leading to aggregation of HNRNPA2/B1 and TARDBP. Interestingly, *PPIA*^{-/-} mice present insoluble proteins with the biochemical features of protein inclusions typical of human TARDBP/TDP-43 proteinopathies (Mackenzie *et al.*, 2007; Kim *et al.*, 2013). Moreover, increased detergent-insolubility of stress granule constituents, such as TARDBP and HNRNPA2/B1, is also indicative of stress granule accumulation (Wolozin, 2012). There is emerging evidence that ALS, FTLN and other degenerative diseases are possibly caused by the inappropriate formation and persistence of stress granules (Buchan *et al.*, 2013) and/or defective transport of RNA granules (Alami *et al.*, 2014). We suggest that PPIA by keeping TARDBP/hnRNP proteins soluble regulates the dynamics and trafficking of mRNP granules. Finally, we propose that *PPIA*^{-/-} mice might serve as a useful model to study TARDBP aggregation. Previous characterization of these mice did not detect any gross behavioural abnormalities (Colgan *et al.*, 2004). However, no detailed study of the neurological phenotype has been done. This analysis is in progress in our laboratory.

PPIA governs TARDBP functions

We tested whether PPIA affected the expression of HDAC6, ATG7, VCP, PGRN, and FUS that are known TARDBP RNA targets with implications for pathogenesis (Fiesel *et al.*, 2010; Bose *et al.*, 2011; Polymenidou *et al.*, 2011; Sephton *et al.*, 2011). HDAC6 is essential for autophagosome-lysosome fusion and protein aggregate clearance (Lee *et al.*, 2010). TARDBP directly binds *HDAC6* mRNA within the coding region and is necessary to maintain its physiological level (Fiesel *et al.*, 2010; Kim *et al.*, 2010). *HDAC6* downregulation after *TARDBP* silencing was associated with impaired cellular turnover of aggregating proteins and reduced neurite outgrowth (Fiesel *et al.*,

2010, 2011). ATG7 is an E1-like enzyme essential for autophagy (Ohsumi and Mizushima, 2004). It has been shown that TARDBP depletion promoted instability of *ATG7* mRNA, downregulation of the protein and impairment of autophagy with accumulation of polyubiquitinated proteins (Bose *et al.*, 2011). Mutations in *FUS*, *GRN* and *VCP* genes cause ALS and/or FTLN. TARDBP binds to the 3' UTR and introns 6 and 7 of *FUS* mRNA and its depletion in mouse adult brain reduced *Fus* mRNA and protein (Polymenidou *et al.*, 2011). On the other hand, TARDBP has a destabilizing effect on the *GRN* transcript by binding its 3' UTR (Polymenidou *et al.*, 2011; Colombrita *et al.*, 2012). Indeed, TARDBP depletion increased *GRN* protein level, in agreement with previously published data (Colombrita *et al.*, 2012). *VCP* is at the intersection of autophagy and ubiquitin proteasome system (Ju and Weihl, 2010). Its mRNA was slightly downregulated upon *TARDBP* silencing in HEK293 cells (Fiesel *et al.*, 2010), consistent with our data at a protein level. The molecular events underlying TARDBP-dependent gene expression regulation are still largely undefined, and likely vary depending on the specific RNA target, cell type and physiological or pathological conditions. In this work we demonstrated that PPIA or TARDBP depletion affected protein levels of HDAC6, ATG7, VCP, GRN, and FUS, in the same way. This suggests that, at least for these genes, PPIA and TARDBP act in a common pathway, where TARDBP is possibly a substrate of PPIA. Interestingly, it has been reported that PPIA enhances hepatitis C virus replication, stimulating the RNA binding ability of the NS5A protein (Foster *et al.*, 2011). Similarly, PPIA could influence the TARDBP binding to its RNA targets. Indeed, we found that PPIA increased the binding of TARDBP to (UG)₁₀ and that this effect depended on PPIase activity. Potentially, a proline-dependent conformational switch, demonstrated for other PPIA substrates (Brazin *et al.*, 2002; Sarkar *et al.*, 2007), could be a novel regulatory mechanism of TARDBP functions.

We also tested the effect of PPIA on the TARDBP-dependent alternative *POLDIP3* splicing (Fiesel *et al.*, 2012). In this case, TARDBP or PPIA depletion have different effects, indicating that PPIA does not influence this

Figure 6 Continued

the onset (*G93A* on) and end-stage (*G93A* es) of disease. Immunoreactivity was normalized to protein loading and multiplied by the amount of Triton-resistant fraction isolated from the tissue. Data (mean ± SEM, *n* = 3) are percentages of immunoreactivity in control samples (*NtgPPIA*^{+/+}). The levels of insoluble pTARDBP in *PPIA*^{-/-} mice were significantly higher than in *PPIA*^{+/+} mice (two-way ANOVA, for *PPIA* genotype: #*P* = 0.0014). **P* < 0.05 by one-way ANOVA, Bonferroni's *post hoc* test. (B and C) Kaplan-Meier curves for survival length (B) and disease duration (C) of *SOD1*^{G93A}*PPIA*^{+/+} (*n* = 23) and *SOD1*^{G93A}*PPIA*^{-/-} (*n* = 16) mice. There is a significant decrease in survival (*P* < 0.01) and disease duration (*P* < 0.05) for *SOD1*^{G93A}*PPIA*^{-/-} versus *SOD1*^{G93A}*PPIA*^{+/+} mice, as assessed by log-rank Mantel-Cox test (see also Supplementary Table 2). (D–F) *SOD1*^{G93A}*PPIA*^{-/-} mice have reduced performance in the functional tests. *SOD1*^{G93A}*PPIA*^{+/+} (*n* = 23) and *SOD1*^{G93A}*PPIA*^{-/-} (*n* = 16) mice were tested for deficit in Rotarod test (D), grip strength (E) and extension reflex (F). Values are mean ± SEM and are percentage of maximum performance (D and E) and score (F). Data were evaluated by two-way ANOVA for repeated measures. (G–I) The level of HDAC6, ATG7 and VCP was analysed in the Triton-soluble fractions from ventral horn lumbar spinal cord tissues of *SOD1*^{G93A} mice expressing (+/+) or not (-/-) PPIA at the onset of disease by dot blot (G and I) and western blot (H). Immunoreactivity was normalized to protein loading (Red Ponceau). Data (mean ± SEM, *n* = 3) are percentages of immunoreactivity in *SOD1*^{G93A}*PPIA*^{+/+} mice; **P* < 0.05 by Student's *t*-test. See also Supplementary Fig. 5.

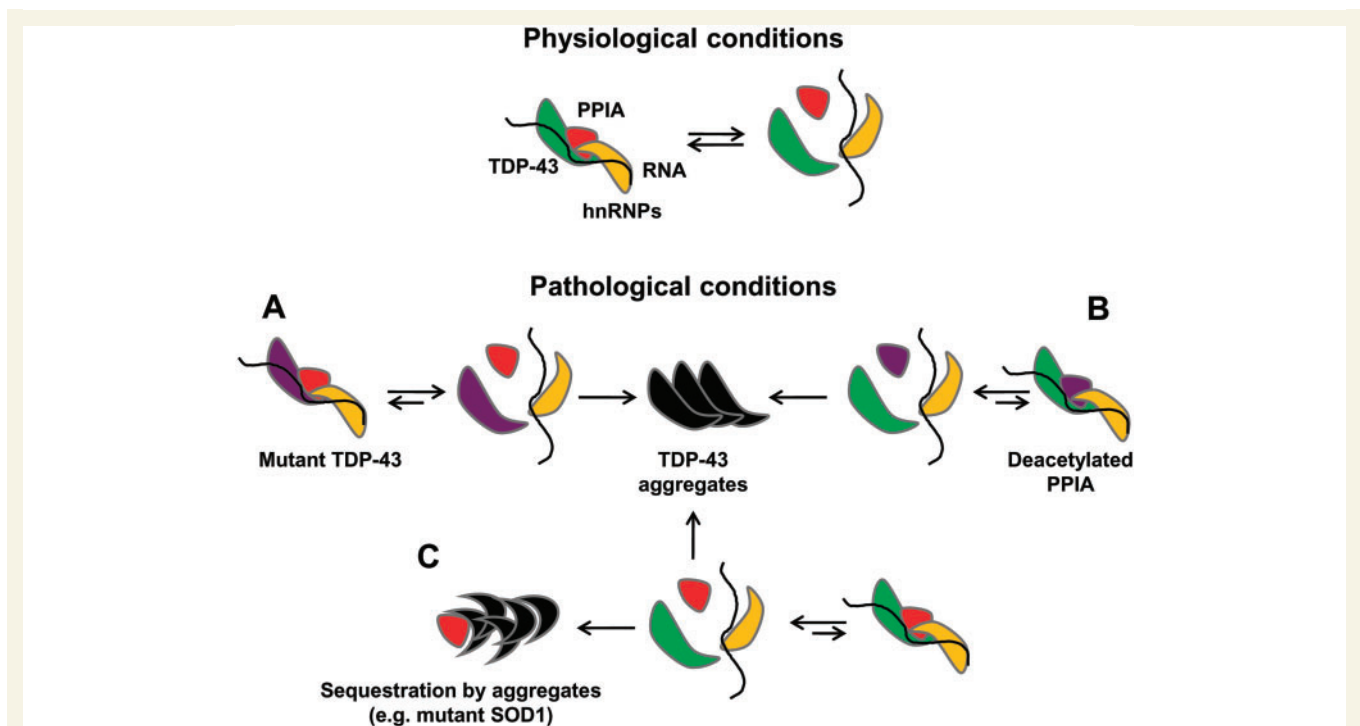


Figure 7 A unifying model to explain TARDBP/TDP-43 pathology. In physiological conditions, PPIA is part of the hnRNP complexes together with TARDBP and other hnRNPs and regulates their dynamic structure. In pathological conditions, (A) mutant TARDBP (TDP-43; possibly also hyper-phosphorylated and/or cleaved) and/or (B) PPIA deacetylation and/or (C) PPIA accidental sequestration into aggregates, while acting as a molecular chaperone, lead to a looser PPIA/TARDBP interaction. This promotes dissociation and instability of the hnRNP complexes, TARDBP mislocalization and aggregation in the cytoplasm. In the case of mutant SOD1, PPIA sequestration in the aggregates and PPIA deacetylation may both contribute to TARDBP pathology. An altered PPIA/TARDBP interaction may affect TARDBP-dependent regulation of genes, such as *HDAC6*, *ATG7* and *VCP*, which are involved in clearance of protein aggregates thus contributing to worsen disease phenotype. A similar mechanism could be envisaged for mutant HNRNPA2/B1 and HNRNPA1, associated with prominent TARDBP pathology (Kim *et al.*, 2013), and interactors of both PPIA (Fig. 1C) (Pan *et al.*, 2008) and TARDBP (Buratti *et al.*, 2005).

TARDBP activity and maybe TARDBP splicing activity in general. It is possible that PPIA and TARDBP interact functionally only within specific hnRNP complexes (not those involved in splicing activity) or the interaction depends on specific TARDBP RNA targets. In view of this fact, it would be interesting to determine a comprehensive TARDBP-RNA interaction map in the presence or absence of PPIA to appreciate the global effect of PPIA on TARDBP putative functions.

The PPIA/TARDBP interaction is impaired in ALS and is a potential therapeutic target

GP-motifs are suggested to be recognition sites for PPIA (Yurchenko *et al.*, 2002; Howard *et al.*, 2003; Piotukh *et al.*, 2005). TARDBP has a single GP-motif (residues 348–349) in the prion-like domain of the protein. Interestingly, mutations in the TARDBP GP-motif, G348C, G348V and G348R, have been associated with familial and sporadic cases of ALS. We found that a

mutation in the TARDBP GP-motif disrupted the interaction with PPIA. However, we cannot exclude that other prolines and most of the C-terminus may be critical. In fact, all the TARDBP pathogenic mutations analysed here substantially reduced the interaction. TARDBP mutants may have lower affinity for PPIA, self-associate through their prion-like domain and accumulate as protein inclusions. Thus, the impaired ability of TARDBP to associate with PPIA may be an important target for therapy, for example through the use of pharmacological chaperones that stabilize the TARDBP structure favouring its interaction with PPIA.

Although deposition of TARDBP is not common in SOD1-linked ALS, recently TARDBP/TDP-43 pathology has also been detected in mutant-SOD1 cases and animal models (Shan *et al.*, 2009; Sumi *et al.*, 2009; Okamoto *et al.*, 2011; Soon *et al.*, 2011; Marino *et al.*, 2015), and our data are consistent with this. In particular, we detected TARDBP mislocalization in HEK293 SOD1^{G93A} cells and in the ventral horn lumbar spinal cord of SOD1^{G93A} mice, where we also found increased detergent-insoluble pTARDBP. The PPIA/TARDBP interaction was impaired

also in mutant-SOD1 experimental models and in the mice at a presymptomatic stage. This is probably the basis of TDP-43 mislocalization and aggregation. Consistent with this model the complete disruption of the PPIA/TARDBP interaction in the *SOD1^{G93A}PPIA^{-/-}* mice increased TARDBP aggregation and hastened disease progression. The absence of PPIA may directly induce TARDBP aggregation and indirectly affect the clearance of protein aggregates by influencing TARDBP-dependent regulation of genes such as *ATG7*, *HDAC6* and *VCP*, which have major roles in autophagy and ubiquitin proteasome system. Interestingly, *VCP* that was only slightly affected by PPIA/TARDBP depletion under physiological conditions, is greatly reduced in *SOD1^{G93A}PPIA^{-/-}* mice, indicating that certain PPIA/TARDBP functions may be activated under pathological conditions. In support of this hypothesis is our recent data showing that in *SOD1^{G93A}* mice with different disease severity, those with slow disease progression show higher soluble levels of PPIA and fewer aggregates in the spinal cord with respect to the fast progressing *SOD1^{G93A}* mice (Marino *et al.*, 2015).

We previously detected changes in the post-translational modification patterns of PPIA in the spinal cord of the *SOD1^{G93A}* mouse at a presymptomatic stage of the disease (Massignan *et al.*, 2007). In this study the same happened in *SOD1^{G93A}* cells and PBMCs of patients with sporadic ALS. Evidence is accumulating that alterations affecting the CNS of patients with ALS are mirrored in PBMCs, including TARDBP mislocalization (De Marco *et al.*, 2011; Nardo *et al.*, 2011). PPIA can undergo different post-translational modifications, including acetylation at different Lys residues (Choudhary *et al.*, 2009). Lys-acetylation at K125 influences key PPIA functions, such as cyclosporin A binding, calcineurin inhibition and HIV-1 capsid interaction (Lammers *et al.*, 2010). Here we found that Lys125 acetylation favoured the interaction with TARDBP, whereas non-acetylated Lys125 did not. We also observed PPIA deacetylation and a decrease in PPIA/TARDBP interaction in *SOD1^{G93A}* cells and in PBMCs of patients with sporadic ALS. Thus deacetylation may cause impaired interaction, and deacetylase inhibitors may be useful as pharmacological tools. It will be important to identify the specific deacetylase involved.

PPIA is sequestered into aggregates and this impedes its interaction with TARDBP

In a previous study we showed that PPIA is one of the protein constituents of Triton-insoluble aggregates isolated from the spinal cord of *SOD1^{G93A}* mice and its level in the Triton-resistant fraction increases as disease progresses (Basso *et al.*, 2009). Here we found that PPIA has preferential affinity for mutant SOD1. We also found an increased amount of insoluble mutant SOD1 in mice knockout for PPIA. This may contribute, together with

increased TARDBP/TDP-43 pathology, to worsen the condition in *SOD1^{G93A}* mice. These data suggest that PPIA could stabilize and refold misfolded SOD1 by direct association, acting as a molecular chaperone. By doing so, it may be accidentally sequestered into mutant SOD1 aggregates. This and PPIA deacetylation could reduce the amount of PPIA available for interaction with TARDBP, destabilizing the hnRNP complexes, leading to TARDBP aggregation and impairing TARDBP functions (Fig. 7). PPIA is enriched in aggregates also isolated from post-mortem tissues of sporadic ALS and FTLN patients (Basso *et al.*, 2009; Seyfried *et al.*, 2012), suggesting that a similar mechanism may be operative in mutant SOD1-independent TARDBP proteinopathies.

Conclusion

We identified a novel function of PPIA that has important implications for the physiology and pathology of the CNS where this protein is highly expressed. PPIA is an interacting partner of TARDBP (also known as TDP-43) and regulates key TARDBP functions, including the regulation of genes involved in clearance of protein aggregates (*HDAC6*, *ATG7* and *VCP*). Disruption of this interaction induces TARDBP aggregation and accelerates disease progression in a mouse model of ALS. Our findings suggest that perturbation of the PPIA/TARDBP interaction equilibrium within the hnRNP complexes, being at the intersection of RNA and protein homeostasis pathways, is the ‘missing link’ of several, apparently unrelated, disorders such as TARDBP/TDP-43 proteinopathies. Targeting the PPIA/TARDBP interaction may represent a novel therapeutic avenue for degenerative conditions involving TARDBP/TDP-43 pathology.

Funding

This work was supported by grants from Telethon Italy (TCR08002 to V.B.), ‘Fondazione Aldo e Cele Dacco’ (to V.B.), the Italian Ministry of Health (CUP E41J12000220001) and the European Community’s Health Seventh Framework Programme (FP7/2007-2013) under grant agreement no. 259867 (to V.B. and C.B). S.P. had a fellowship from ‘Fondazione Vialli e Mauro per la ricerca e lo sport’.

Supplementary material

Supplementary material is available at *Brain* online.

Acknowledgements

We thank Emanuele Buratti and Francisco Baralle (ICGEB, Trieste, Italy) for the anti-TDP-43 antibody and the plasmids expressing Flag-TDP-43^{WT} and Flag-TDP-43^{G348V}.

and Christopher E. Shaw (King's College London, UK), Emma Scotter (The Centre for Brain Research, New Zealand) and Boris Rogelj (Jozef Stefan Institute, Slovenia) for the plasmids expressing HA-TDP-43^{WT} and HA-TDP-43^{ΔRRM1}. We thank Mauro Pignataro for PBMC isolation and Massimo Tortarolo for preparation of spinal neuron cultures. Roberto Chiesa and Emiliano Biasini kindly offered useful discussion and advice on how to write up the manuscript. We thank Mario Salmona for fruitful discussions and Judith Baggott for editorial assistance.

References

- Alami NH, Smith RB, Carrasco MA, Williams LA, Winborn CS, Han SS, et al. Axonal transport of TDP-43 mRNA granules is impaired by ALS-causing mutations. *Neuron* 2014; 81: 536–43.
- Atkin JD, Farg MA, Turner BJ, Tomas D, Lysaght JA, Nunan J, et al. Induction of the unfolded protein response in familial amyotrophic lateral sclerosis and association of protein-disulfide isomerase with superoxide dismutase 1. *J Biol Chem* 2006; 281: 30152–65.
- Basso M, Massignan T, Samengo G, Cheroni C, De Biasi S, Salmona M, et al. Insoluble mutant SOD1 is partly oligoubiquitinated in amyotrophic lateral sclerosis mice. *J Biol Chem* 2006; 281: 33325–35.
- Basso M, Pozzi S, Tortarolo M, Fiordaliso F, Bisighini C, Pasetto L, et al. Mutant copper-zinc superoxide dismutase (SOD1) induces protein secretion pathway alterations and exosome release in astrocytes: implications for disease spreading and motor neuron pathology in amyotrophic lateral sclerosis. *J Biol Chem* 2013; 288: 15699–711.
- Basso M, Samengo G, Nardo G, Massignan T, D'Alessandro G, Tartari S, et al. Characterization of detergent-insoluble proteins in ALS indicates a causal link between oxidative stress and aggregation in pathogenesis. *PLoS One* 2009; 4: e8130.
- Bendotti C, Marino M, Cheroni C, Fontana E, Crippa V, Poletti A, et al. Dysfunction of constitutive and inducible ubiquitin-proteasome system in amyotrophic lateral sclerosis: implication for protein aggregation and immune response. *Prog Neurobiol* 2012; 97: 101–26.
- Bose JK, Huang CC, Shen CK. Regulation of autophagy by neuro-pathological protein TDP-43. *J Biol Chem* 2011; 286: 44441–8.
- Brazin KN, Mallis RJ, Fulton DB, Andreotti AH. Regulation of the tyrosine kinase Itk by the peptidyl-prolyl isomerase cyclophilin A. *Proc Natl Acad Sci USA* 2002; 99: 1899–904.
- Buchan JR, Kolaitis RM, Taylor JP, Parker R. Eukaryotic stress granules are cleared by autophagy and Cdc48/VCP function. *Cell* 2013; 153: 1461–74.
- Budini M, Buratti E, Stuani C, Guarnaccia C, Romano V, De Conti L, et al. Cellular model of TAR DNA-binding protein 43 (TDP-43) aggregation based on its C-terminal Gln/Asn-rich region. *J Biol Chem* 2012; 287: 7512–25.
- Buratti E, Baralle FE. The multiple roles of TDP-43 in pre-mRNA processing and gene expression regulation. *RNA Biol* 2010; 7: 420–9.
- Buratti E, Brindisi A, Giombi M, Tisminetzky S, Ayala YM, Baralle FE. TDP-43 binds heterogeneous nuclear ribonucleoprotein A/B through its C-terminal tail: an important region for the inhibition of cystic fibrosis transmembrane conductance regulator exon 9 splicing. *J Biol Chem* 2005; 280: 37572–84.
- Casoni F, Basso M, Massignan T, Gianazza E, Cheroni C, Salmona M, et al. Protein nitration in a mouse model of familial amyotrophic lateral sclerosis: possible multifunctional role in the pathogenesis. *J Biol Chem* 2005; 280: 16295–304.
- Chen S, Zhang X, Song L, Le W. Autophagy dysregulation in amyotrophic lateral sclerosis. *Brain Pathol* 2012; 22: 110–6.
- Choudhary C, Kumar C, Gnäd F, Nielsen ML, Rehman M, Walther TC, et al. Lysine acetylation targets protein complexes and co-regulates major cellular functions. *Science* 2009; 325: 834–40.
- Colgan J, Asmal M, Neagu M, Yu B, Schneidkraut J, Lee Y, et al. Cyclophilin A regulates TCR signal strength in CD4+ T cells via a proline-directed conformational switch in Itk. *Immunity* 2004; 21: 189–201.
- Colombrita C, Onesto E, Megiorni F, Pizzuti A, Baralle FE, Buratti E, et al. TDP-43 and FUS RNA-binding proteins bind distinct sets of cytoplasmic messenger RNAs and differently regulate their post-transcriptional fate in motoneuron-like cells. *J Biol Chem* 2012; 287: 15635–47.
- D'Ambrogio A, Buratti E, Stuani C, Guarnaccia C, Romano M, Ayala YM, et al. Functional mapping of the interaction between TDP-43 and hnRNP A2 *in vivo*. *Nucleic Acids Res* 2009; 37: 4116–26.
- De Marco G, Lupino E, Calvo A, Moglia C, Buccinna B, Grifoni S, et al. Cytoplasmic accumulation of TDP-43 in circulating lymphomonocytes of ALS patients with and without TARDBP mutations. *Acta Neuropathol* 2011; 121: 611–22.
- Dreyfuss G, Kim VN, Kataoka N. Messenger-RNA-binding proteins and the messages they carry. *Nat Rev Mol Cell Biol* 2002; 3: 195–205.
- Fiesel FC, Schurr C, Weber SS, Kahle PJ. TDP-43 knockdown impairs neurite outgrowth dependent on its target histone deacetylase 6. *Mol Neurodegener* 2011; 6: 64.
- Fiesel FC, Voigt A, Weber SS, Van den Haute C, Waldenmaier A, Gorner K, et al. Knockdown of transactive response DNA-binding protein (TDP-43) downregulates histone deacetylase 6. *EMBO J* 2010; 29: 209–21.
- Fiesel FC, Weber SS, Supper J, Zell A, Kahle PJ. TDP-43 regulates global translational yield by splicing of exon junction complex component SKAR. *Nucleic Acids Res* 2012; 40: 2668–82.
- Fischer G, Wittmann-Liebold B, Lang K, Kiefhaber T, Schmid FX. Cyclophilin and peptidyl-prolyl cis-trans isomerase are probably identical proteins. *Nature* 1989; 337: 476–8.
- Foster TL, Gallay P, Stonehouse NJ, Harris M. Cyclophilin A interacts with domain II of hepatitis C virus NS5A and stimulates RNA binding in an isomerase-dependent manner. *J Virol* 2011; 85: 7460–4.
- Freibaum BD, Chitta RK, High AA, Taylor JP. Global analysis of TDP-43 interacting proteins reveals strong association with RNA splicing and translation machinery. *J Proteome Res* 2010; 9: 1104–20.
- Freskgard PO, Bergenhem N, Jonsson BH, Svensson M, Carlsson U. Isomerase and chaperone activity of prolyl isomerase in the folding of carbonic anhydrase. *Science* 1992; 258: 466–8.
- Howard BR, Vajdos FF, Li S, Sundquist WI, Hill CP. Structural insights into the catalytic mechanism of cyclophilin A. *Nat Struct Biol* 2003; 10: 475–81.
- Ju JS, Wehl CC. p97/VCP at the intersection of the autophagy and the ubiquitin proteasome system. *Autophagy* 2010; 6: 283–5.
- Kim HJ, Kim NC, Wang YD, Scarborough EA, Moore J, Diaz Z, et al. Mutations in prion-like domains in hnRNPA2B1 and hnRNPA1 cause multisystem proteinopathy and ALS. *Nature* 2013; 495: 467–73.
- Kim SH, Shanware NP, Bowler MJ, Tibbetts RS. Amyotrophic lateral sclerosis-associated proteins TDP-43 and FUS/TLS function in a common biochemical complex to co-regulate HDAC6 mRNA. *J Biol Chem* 2010; 285: 34097–105.
- Kirby J, Goodall EF, Smith W, Highley JR, Masanzu R, Hartley JA, et al. Broad clinical phenotypes associated with TAR-DNA binding protein (TARDBP) mutations in amyotrophic lateral sclerosis. *Neurogenetics* 2010; 11: 217–25.
- Lammers M, Neumann H, Chin JW, James LC. Acetylation regulates cyclophilin A catalysis, immunosuppression and HIV isomerization. *Nat Chem Biol* 2010; 6: 331–7.

- Lee JY, Koga H, Kawaguchi Y, Tang W, Wong E, Gao YS, et al. HDAC6 controls autophagosome maturation essential for ubiquitin-selective quality-control autophagy. *EMBO J* 2010; 29: 969–80.
- Ling SC, Polymenidou M, Cleveland DW. Converging mechanisms in ALS and FTD: disrupted RNA and protein homeostasis. *Neuron* 2013; 79: 416–38.
- Mackenzie IR, Bigio EH, Ince PG, Geser F, Neumann M, Cairns NJ, et al. Pathological TDP-43 distinguishes sporadic amyotrophic lateral sclerosis from amyotrophic lateral sclerosis with SOD1 mutations. *Ann Neurol* 2007; 61: 427–34.
- Mackenzie IR, Rademakers R, Neumann M. TDP-43 and FUS in amyotrophic lateral sclerosis and frontotemporal dementia. *Lancet Neurol* 2010; 9: 995–1007.
- Marino M, Papa S, Crippa V, Nardo G, Peviani M, Cheroni C, et al. Differences in protein quality control correlate with phenotype variability in 2 mouse models of familial amyotrophic lateral sclerosis. *Neurobiol Aging* 2015; 36: 492–504.
- Massignan T, Casoni F, Basso M, Stefanazzi P, Biasini E, Tortarolo M, et al. Proteomic analysis of spinal cord of presymptomatic amyotrophic lateral sclerosis G93A SOD1 mouse. *Biochem Biophys Res Commun* 2007; 353: 719–25.
- Nardo G, Pozzi S, Mantovani S, Garbelli S, Marinou K, Basso M, et al. Nitroproteomics of peripheral blood mononuclear cells from patients and a rat model of ALS. *Antioxid Redox Signal* 2009; 11: 1559–67.
- Nardo G, Pozzi S, Pignataro M, Lauranzano E, Spano G, Garbelli S, et al. Amyotrophic lateral sclerosis multiprotein biomarkers in peripheral blood mononuclear cells. *PLoS One* 2011; 6: e25545.
- Neumann M, Sampathu DM, Kwong LK, Truax AC, Micsenyi MC, Chou TT, et al. Ubiquitinated TDP-43 in frontotemporal lobar degeneration and amyotrophic lateral sclerosis. *Science* 2006; 314: 130–3.
- Nigro P, Pompilio G, Capogrossi MC. Cyclophilin A: a key player for human disease. *Cell Death Dis* 2013; 4: e888.
- Ohsumi Y, Mizushima N. Two ubiquitin-like conjugation systems essential for autophagy. *Semin Cell Dev Biol* 2004; 15: 231–6.
- Okamoto Y, Ihara M, Urushitani M, Yamashita H, Kondo T, Tanigaki A, et al. An autopsy case of SOD1-related ALS with TDP-43 positive inclusions. *Neurology* 2011; 77: 1993–5.
- Pan H, Luo C, Li R, Qiao A, Zhang L, Mines M, et al. Cyclophilin A is required for CXCR4-mediated nuclear export of heterogeneous nuclear ribonucleoprotein A2, activation and nuclear translocation of ERK1/2, and chemotactic cell migration. *J Biol Chem* 2008; 283: 623–37.
- Pappin DJ, Hojrup P, Bleasby AJ. Rapid identification of proteins by peptide-mass fingerprinting. *Curr Biol* 1993; 3: 327–32.
- Phukan J, Elamin M, Bede P, Jordan N, Gallagher L, Byrne S, et al. The syndrome of cognitive impairment in amyotrophic lateral sclerosis: a population-based study. *J Neurol Neurosurg Psychiatry* 2012; 83: 102–8.
- Piotukh K, Gu W, Kofler M, Labudde D, Helms V, Freund C. Cyclophilin A binds to linear peptide motifs containing a consensus that is present in many human proteins. *J Biol Chem* 2005; 280: 23668–74.
- Polymenidou M, Lagier-Tourenne C, Hutt KR, Huelga SC, Moran J, Liang TY, et al. Long pre-mRNA depletion and RNA missplicing contribute to neuronal vulnerability from loss of TDP-43. *Nat Neurosci* 2011; 14: 459–68.
- Robberecht W, Philips T. The changing scene of amyotrophic lateral sclerosis. *Nat Rev Neurosci* 2013; 14: 248–64.
- Ryffel B, Woerly G, Greiner B, Haendler B, Mihatsch MJ, Foxwell BM. Distribution of the cyclosporine binding protein cyclophilin in human tissues. *Immunology* 1991; 72: 399–404.
- Sarkar P, Reichman C, Saleh T, Birge RB, Kalodimos CG. Proline cis-trans isomerization controls autoinhibition of a signaling protein. *Mol Cell* 2007; 25: 413–26.
- Sephton CF, Cenik C, Kucukural A, Dammer EB, Cenik B, Han Y, et al. Identification of neuronal RNA targets of TDP-43-containing ribonucleoprotein complexes. *J Biol Chem* 2011; 286: 1204–15.
- Seyfried NT, Gozal YM, Donovan LE, Herskowitz JH, Dammer EB, Xia Q, et al. Quantitative analysis of the detergent-insoluble brain proteome in frontotemporal lobar degeneration using SILAC internal standards. *J Proteome Res* 2012; 11: 2721–38.
- Shan X, Vocadlo D, Krieger C. Mislocalization of TDP-43 in the G93A mutant SOD1 transgenic mouse model of ALS. *Neurosci Lett* 2009; 458: 70–4.
- Soon CP, Donnelly PS, Turner BJ, Hung LW, Crouch PJ, Sherratt NA, et al. Diacetylbis(N(4)-methylthiosemicarbazonato) copper(II) (CuII(atms)) protects against peroxynitrite-induced nitrosative damage and prolongs survival in amyotrophic lateral sclerosis mouse model. *J Biol Chem* 2011; 286: 44035–44.
- Sumi H, Kato S, Mochimaru Y, Fujimura H, Etoh M, Sakoda S. Nuclear TAR DNA binding protein 43 expression in spinal cord neurons correlates with the clinical course in amyotrophic lateral sclerosis. *J Neuropathol Exp Neurol* 2009; 68: 37–47.
- Thomas M, Alegre-Abarrategui J, Wade-Martins R. RNA dysfunction and aggregate pathology at the centre of an amyotrophic lateral sclerosis/frontotemporal dementia disease continuum. *Brain* 2013; 136: 1345–60.
- Wolozin B. Regulated protein aggregation: stress granules and neurodegeneration. *Mol Neurodegener* 2012; 7: 56.
- Yurchenko V, Zybarth G, O'Connor M, Dai WW, Franchin G, Hao T, et al. Active site residues of cyclophilin A are crucial for its signaling activity via CD147. *J Biol Chem* 2002; 277: 22959–65.
- Zydowsky LD, Etzkorn FA, Chang HY, Ferguson SB, Stolz LA, Ho SI, et al. Active site mutants of human cyclophilin A separate peptidyl-prolyl isomerase activity from cyclosporin A binding and calcineurin inhibition. *Protein Sci* 1992; 1: 1092–9.